THE INTERNATIONAL JOURNAL OF MEDICAL ROBOTICS AND COMPUTER ASSISTED SURGERY
Int J Med Robotics Comput Assist Surg 2007; **3**: 140–148.
Published online in Wiley InterScience (www.interscience.wiley.com). **DOI:** 10.1002/rcs.136

ORIGINAL ARTICLE

Minimization of needle deflection in robot-assisted percutaneous therapy

Niki Abolhassani[1,2]*
Rajni V. Patel[1,2]
Farzam Ayazi[3]

[1]*Canadian Surgical Technologies and Advanced Robotics (CSTAR), London, Ontario, Canada*

[2]*Department of Electrical and Computer Engineering, University of Western Ontario, London, Ontario, Canada*

[3]*Lawson Health Research Institute, London, Ontario, Canada*

*Correspondence to:
Niki Abolhassani, Department of Electrical and Computer Engineering, University of Western Ontario, 1151 Richmond Street North, London, Ontario, Canada N6A 5B9. E-mail: nabolhas@uwo.ca

Accepted: 2 May 2007

Abstract

Background Needle deflection and tissue deformation are two problems encountered during needle insertion into soft, non-homogeneous tissue. They affect the accuracy of needle placement, which in turn affects the effectiveness of needle-based therapies and biopsies.

Methods In this study, a needle is inserted using a robot with two degrees of freedom. The needle is modelled as a flexible beam with clamped support at one end, and its deflection is estimated using online force/moment measurements at the needle base. To compensate for the needle deflection, the needle is axially rotated through 180°. The needle deflection estimation data is used to find the insertion depths at which needle rotations are to be performed.

Results A bevelled-tip needle was inserted into animal tissue. The needle deflection at the target was reduced by about 90%. It was observed that minimization of needle deflection reduced tissue deformation. The proposed method reduced needle deflection more than when needle insertion was performed with constant rotation.

Conclusions Estimating needle tip position using online force/moment measurement improves the accuracy of robot-assisted percutaneous procedures when imaging feedback is not available.

Keywords robotic needle insertion; prostate brachytherapy; needle deflection; trajectory generation; soft tissue deformation

Introduction

Robot-assisted needle insertion has attracted considerable attention in recent years because of its promising application in minimally invasive percutaneous procedures such as biopsies and brachytherapies (1). In robot-assisted needle insertions, a robot is used to guide a needle through a particular path and place the needle tip at a certain target. The main complication in these procedures is due to tissue deformation and needle deflection, which change the needle track and cause displacement of the target. Such changes reduce the effectiveness of the therapy and/or precision of diagnosis (2). In procedures such as prostate brachytherapy, which involves the permanent implantation of radioactive seeds within the prostate gland, the track of the needle shaft inside the tissue is as important as the needle tip placement. The current dosimetry-planning systems are based on straight parallel tracks for the needles (Figure 1). Intramediastinal or intra-

abdominal biopsies and abscess draining are examples of medical applications that use the flexibility of the needle in order to create curvatures along the path so as to avoid possible obstacles or anatomical structures (3,4).

In percutaneous therapies, an imaging system is generally used to provide visual feedback to the clinician while the clinician navigates the tool inside the patient's body (5–7). In robot-assisted percutaneous procedures, the imaging system could provide information regarding the needle tip position and tissue movement for monitoring and control of the robot motion. However, there are major limitations with regard to visual feedback along the insertion path in interventional procedures, such as unavailability of imaging data during part of the insertion path and/or lack of a high resolution three-dimensional (3D) real-time imaging system. For example, in trans-rectal ultrasound (TRUS) prostate brachytherapy, there is a region from the skin to the neighbourhood of the prostate where imaging data is not provided while the needle is being inserted (connective tissue area in Figure 1). Therefore, other techniques are required to control the needle motion within this region. This study was initiated for steering the needle such that the shaft remains as straight as possible along the needle insertion path within this region. We describe a model to estimate the amount of needle deflection during insertion without imaging feedback and propose a trajectory-generation algorithm that allows straight insertion of the needle using a robot with two degrees of freedom (DOF).

Past work has shown that deflection of flexible long needles is caused by the geometry of the needle tip and the mechanical properties of soft tissue (8,9). Tissue deformation and needle deflection can both affect the net amount of needle tip displacement. Tissue deformation is due to the mechanical properties of soft tissue and frictional forces between the needle shaft and the tissue. Needle rotation and control of needle velocity based on force data are some suggested solutions to reduce tissue deformation (10). The effects of high-speed needle rotation and orientation reversal at half of the insertion depth have also been shown to increase the accuracy of targeting (11). Kataoka *et al.* (9) have proposed a model for force deflection of a bevelled-tip needle during insertion. Their model uses only the transverse force of the needle base to predict the amount of needle deflection. They found that the slope of displacement vs. length at different needle diameters was comparable; however, the predicted deflection was smaller than the measured deflection.

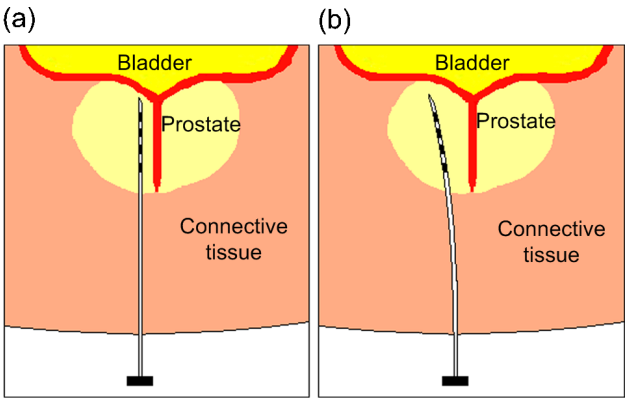

Figure 1. Needle deflection affects the placement of the seeds to be implanted. (a) Seeds location without needle deflection. (b) Seeds location when the needle is deflected. In TRUS prostate brachytherapy, an ultrasound probe is inserted in the patient's rectum and is locked in place. The TRUS probe can only scan the neighbourhood of the prostate, not the entire insertion path

Most recent studies are focused on insertion of the needle into synthesized material. DiMaio and Salcudean (12,13) presented a method for steering a needle into a very soft tissue phantom made of PVC. In their approach, the tissue was moved by steering the needle base outside the tissue and the tissue deformation helped to avoid the obstacles. In contrast, Webster *et al.* (14) assumed no tissue deformation during insertion and developed a model for steering bevel-tipped needles in a rubber-like simulated muscle (relatively hard tissue). They used the model to control the needle motion by assuming a constant curvature for the needle path. Their study required the curvature constant to be known for the phantom prior to insertion. The predefined curvature constant approach was also combined with a numerical optimization algorithm for needle rotation in a simulation application, in order to steer the needle while avoiding obstacles (15). Alterovitz *et al.* (15) assumed that 'the tissue is stiff relative to the needle and that the needle is thin, sharp and low-friction, so the tissue does not significantly deform'. Our approach is different from the past work, as real-time force/moment readings at the needle base are used to estimate the amount of needle deflection and to compensate for it by rotating the needle. To the best of our knowledge, no other group has ever presented a reliable method for real-time estimation of needle deflection and curvature constant in soft tissue without a need for a position sensor. Moreover, we present the effect of the proposed algorithm on tissue deformation and compare the effect of different insertions on needle deflection. The scope of this paper does not include tissue modelling and compensation for tissue deformation; however, we would like to ensure that the proposed algorithm is not causing more tissue deformation.

Methodology

Experimental set-up

A test-bed has been set up in our laboratory for studying needle insertion in soft tissue. As shown in Figure 2, a 2-DOF robot with a needle attached as its tool is used for this study. The robot provides translation in one (horizontal) direction and rotation about the translational axis. Needle insertion is performed using the translational motion. The axial rotation is added to study its effect on needle deflection while the needle is being inserted into soft tissue. A 6-DOF force/torque sensor (Nano43, ATI

DOI: 10.1002/rcs

Industrial Automation) is attached to the needle holder to measure the forces and moments acting on the needle. In order to track the needle tip position in 3D during insertion, a sensor coil (Figure 3) is inserted inside the needle and is secured very close to the needle tip. The 5-DOF sensor coil is part of the Aurora magnetic tracking system from Northern Digital Inc. (NDI) that is used in the experiments. The Aurora magnetic tracking system shows improved performance in the presence of small metal objects, compared to earlier versions of magnetic tracking technology. The needle and needle holder material appear to have negligible effect on the tracking accuracy of the system. Magnetic sensors are used instead of an imaging system in order to acquire 3D needle tip position data at the same rate as the force readings (500 Hz). A high-resolution real-time ultrasound system which can measure needle position during the entire insertion at such a rate was not available. It should be noted that the sensor coil measurements are used for validating the results, rather than controlling the needle tip position. In order to validate the performance of the proposed method with regard to tissue deformation, image data are acquired before and after each insertion. A camera from Point Grey Research Inc. is used to obtain images of needle deflection at the tissue entry point and a Philips iU22 ultrasound system is used for studying internal tissue deformation.

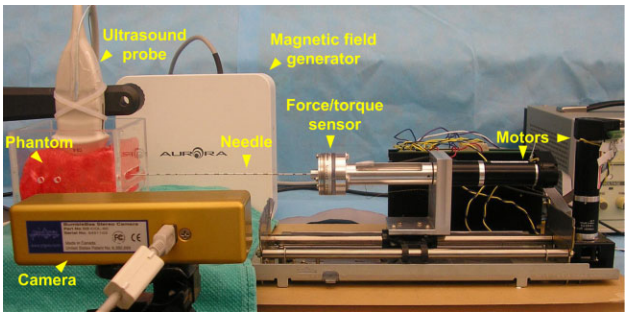

Figure 2. The experimental set-up with a phantom. One lens of the camera was aligned for grabbing images from the needle at entry point to the tissue

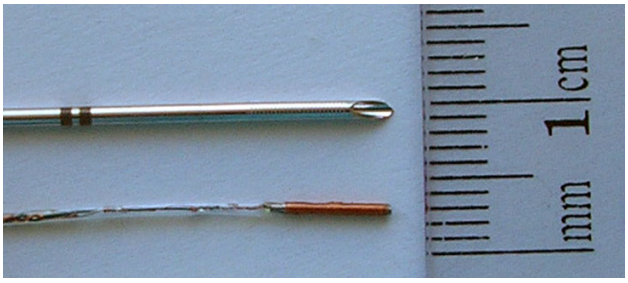

Figure 3. Sensor coil and needle

A multi-threaded application (called NeedleController) for position/velocity control, force/torque reading, magnetic sensor tracking and image data acquisition has been developed using Microsoft® Foundation Class (MFC) in Visual C++. This application runs on a Pentium 4, 2.4 GHz computer, with Microsoft® Windows 2000 as its operating system. The NeedleController application has a graphical user interface (GUI) which enables the user to define the speed and depth of insertion as well as the speed and direction of needle rotation and to monitor needle insertion (Figure 4). A proportional-integral-derivative (PID) control scheme has been developed to control the needle motion in order to track specified trajectories in both degrees of freedom during needle insertion. Position data used for motion control are obtained from encoder readings. The experiments were carried out on excised animal tissue.

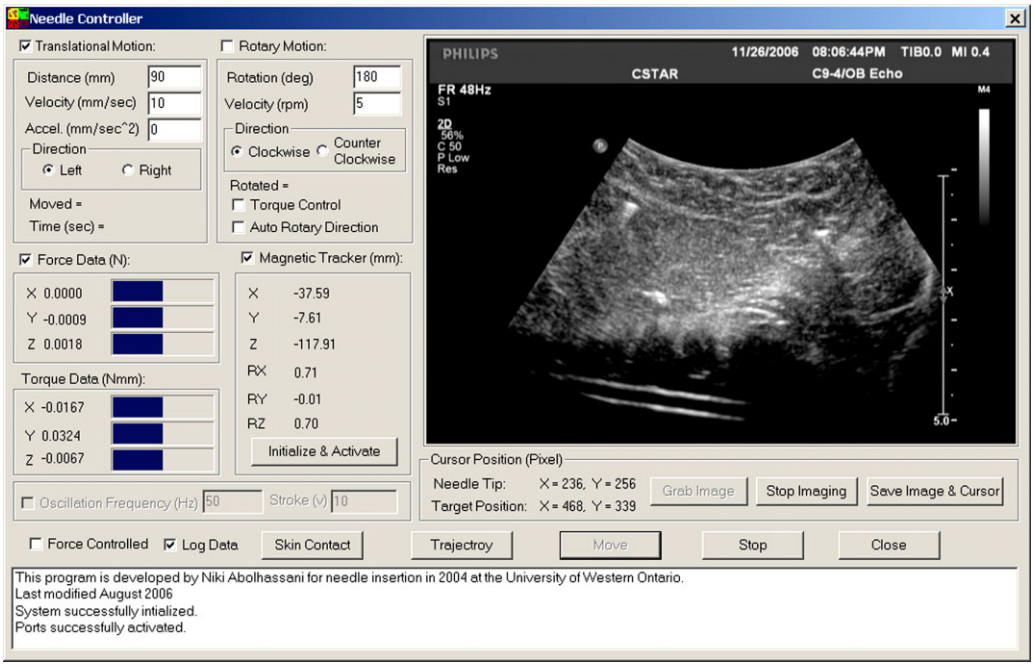

Figure 4. The NeedleController GUI

DOI: 10.1002/rcs

Needle deflection estimation

For accurate needle insertion, it is desirable to calculate the magnitude of deflection orthogonal to the insertion direction and to compensate for it. It is known that a bevelled-tip needle deflects towards the direction of the bevel, due to the asymmetric forces acting on the tip of the needle (14,15). This deflection causes a curved path for the needle shaft inside the tissue. In order to estimate the amount of needle deflection during insertion, we consider the needle as a flexible prismatic beam with clamped support at the base and find the relationship between the needle tip deflection and forces and moments acting on the needle (Figure 5a).

It should be noted that Figure 5a shows an exaggerated deflection curve for the needle with respect to its insertion depth. In fact, the deflection curve of the needle has a very small slope ($dv/dz \ll 1$) and as such the vertical component of the stick-slip friction force is negligible, and also the expression for the curvature (16) can be simplified as:

$$\frac{1}{\rho} = \frac{d^2v}{dz^2} \tag{1}$$

Since the needle is considered to be at equilibrium at each instant:

$$\sum F_{vertical} = 0 \Rightarrow -F_c \cos\theta + F_r + q_0(L - L_o)/2 = 0 \tag{2}$$

$$\sum M_{base} = 0 \Rightarrow M_r - F_c L \cos\theta + q_0(L^2 - 2{L_o}^2 + LL_o)/6 = 0 \tag{3}$$

where $\theta, F_c, F_r, M_r, q_0, L,$ and L_o are the angle of the bevel, the cutting force at the tip, the vertical reaction force measured at the needle base, the reaction moment at the clamped needle base, the maximum intensity of the triangularly distributed resistance force, the total needle length and the needle length outside the tissue, respectively. To determine the equation of the deflection curve for the needle, we use the bending-moment equation (16), defined by:

$$\frac{M}{EI} = \frac{d^2v}{dz^2} \tag{4}$$

where E is the Young's modulus of the needle, I is the area moment of inertia, M and v are the internal moment and deflection at a distance z from the needle base in the Z direction. The bending moment of the needle at a distance z from the base is obtained from the free-body diagrams (Figure 5b, c) and can be written as:

$$M = M_r - F_r z \quad \text{if } (0 \le z \le L_o) \tag{5}$$

$$M = M_r - F_r z - q_0(3L - z - 2L_o)(z - L_o)^2/6(L - L_o) \quad \text{if } (L_o \le z \le L) \tag{6}$$

where F_r and M_r are measured at the base of the needle using the 6-DOF force/torque sensor. According to equation 4, the amount of deflection at a distance z from the needle base can be calculated by twice integration of equations 5 and 6 and q_0 can be obtained using equations 2 and 3.

In our set-up, there is no external lateral force from the needle base to cause tissue deformation and the needle cuts the tissue as it penetrates into it. It is observed that at the entry point, the tissue stiffness is not high enough to prevent the tissue from movement in the direction of deflection. Since the last term of equation 6, after twice integration at the needle tip ($z = L$), was found to be very small, this term can be neglected and equation 5 can be used for calculating the bending moment at any point z along the needle. Therefore, the actual amount of deflection at the needle tip can be calculated using:

$$v = \sum_{i=0}^{n} (3\Delta M_{r_i} L^2 - \Delta F_{r_i} L^3)/6EI \tag{7}$$

where n is the number of steps to reach a certain depth inside the tissue and ΔM_{r_i} and ΔF_{r_i} are changes in the amount of moment and force values between two consecutive steps. In equation 7, the amount of deflection is obtained from a small-scale model obtained from linearization. This model removes the dependency of the force and moment values on the insertion depth, i.e. they can be considered constant over small insertion depths. Using equations 1 and 7, the radius of the needle curvature can be calculated.

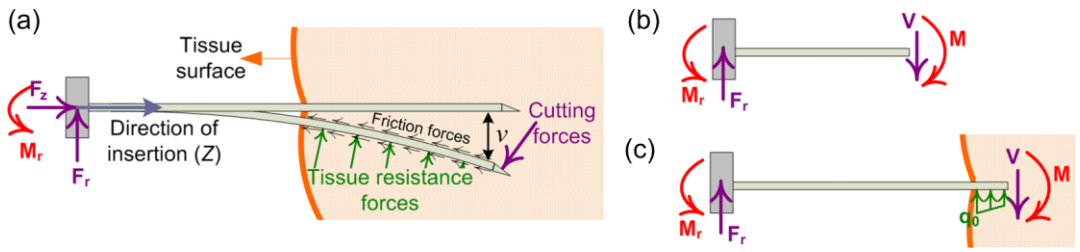

Figure 5. Needle deflection v in 2D plane. (a) Forces acting on the needle. (b) Shear force V and bending moment M at a cross-section just to the left of the tissue surface. (c) Shear force and bending moment at a cross-section just to the right of the tissue surface (inside tissue). Tissue resistance forces are modelled as triangularly distributed loads with maximum intensity at the entry point

Trajectory generation

The aim of this study was to insert a needle and maintain the needle shaft as straight as possible during insertion into soft tissue. It is suggested that needle deflection can be compensated by rotating the needle through 180° when the deflection goes beyond a pre-defined tolerance (17). A rotation of 180° causes the bevel at the needle tip to point in the opposite direction to the preceding direction of deflection and thereby reduces the needle deflection from the insertion path. During all insertions, the trajectory is generated such that the needle is moved with constant translational velocity. Whenever needle rotation is required, the translational motion of the needle is paused, and is resumed after the 180° rotation is completed.

To determine the location at which needle rotation is to be performed, we use the estimation model presented by equation 7 to find the amount of needle deflection at each time step. When the amount of the estimated deflection reaches a pre-defined (acceptable) threshold, the needle is rotated. Thereafter, the needle tip position is predicted using the uniform motion along a circular segment with curvature ρ that is calculated prior to the first rotation, using equations 1 and 7. Rotation of the needle for 180° causes a change in the direction of motion on the circular segment (15). Figure 6 shows how the needle curvature is affected by needle rotations.

Depending on the tissue type and the depth of insertion, it may be necessary to rotate the needle at several points along the trajectory to keep the needle as straight as possible or to reach a particular target. After the first rotation, motion of the needle along the circular segment is used to predict when the needle deflection goes beyond its limit. Figure 7 explains the required steps

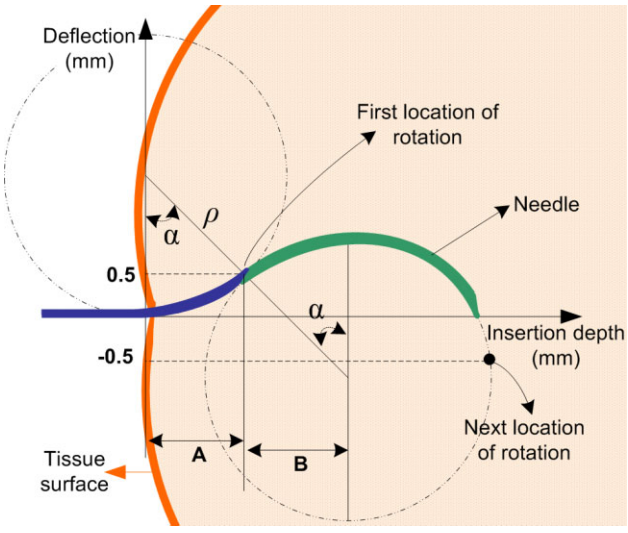

Figure 6. Motion of a needle along a circular segment during insertion. The radius of the circular segment is ρ and α is the deflection angle prior to each rotation. Part A is the insertion distance prior to the first needle rotation; part B is the insertion distance during which the needle deflection increases after each rotation

for generating and updating the trajectory for inserting one needle. The data obtained from each insertion can be used to refine the curvature value and also to optimize the deflection threshold used for needle rotation in subsequent insertions.

Moreover, during needle insertion and rotation, a torsional stress exists on the needle shaft, which could change the orientation angle of the bevelled tip. This change in the orientation angle could affect the direction of needle deflection. Therefore, the value of the twisting torque is used to adjust the amount of needle rotation. The twisting angle is calculated (16) using:

$$\phi = T_z L \Big/ JG \tag{8}$$

where T_z is the torque measured at the needle base in the insertion direction and L, J and G are the length, the polar moment and the shear modulus of the needle, respectively.

Finally, two other trajectories were generated to compare their effects on needle deflection with the proposed method: insertion with no rotation, and insertion with high-speed needle rotation (needle spinning).

Tissue deformation measurement

The method presented here deals explicitly with the problem of needle deflection during insertion into soft tissue. However, it is of particular interest to observe whether the method presented can have any effect on the amount of tissue deformation. Tissue deformation is studied from two perspectives: tissue deformation at the entry point of the needle into tissue and tissue deformation inside the tissue at or near a target. Prior to conducting the experiments, the camera and ultrasound (18) images are calibrated. Images are acquired by camera and ultrasound before each insertion, i.e. I_{bc} and I_{bu}, and after each insertion, i.e. I_{ac} and I_{au}. It should be noted that the needle was brought into tissue contact position in order to record I_{bc} and I_{bu}.

To measure the amount of tissue deformation at the entry point, i.e. δ_{entry}, we first apply a landmark rigid registration of I_{bc} on I_{ac}. Then, δ_{entry} is obtained using:

$$\delta_{entry} = v_{entry} = \|\lambda_c (P_{eb} - P_{ea})\| \tag{9}$$

where λ_c is the resolution of the camera obtained from calibration and P_{eb} and P_{ea} are pixel positions of the needle at the entry point in I_{bc} and I_{ac}, respectively. Pixel positions are defined as $[x, y]'$, where x and y define the row and column pixels of a point of interest in a given image. The notation $\|(\cdot)\|$ denotes the Euclidean norm of $(\cdot)$.

To measure the internal tissue deformation at a target, a set of beads and spacers are placed orthogonal to the path of insertion, at the same height as the needle and about 60 mm inside the tissue. For each insertion, the ultrasound probe is adjusted to grab an image from the

DOI: 10.1002/rcs

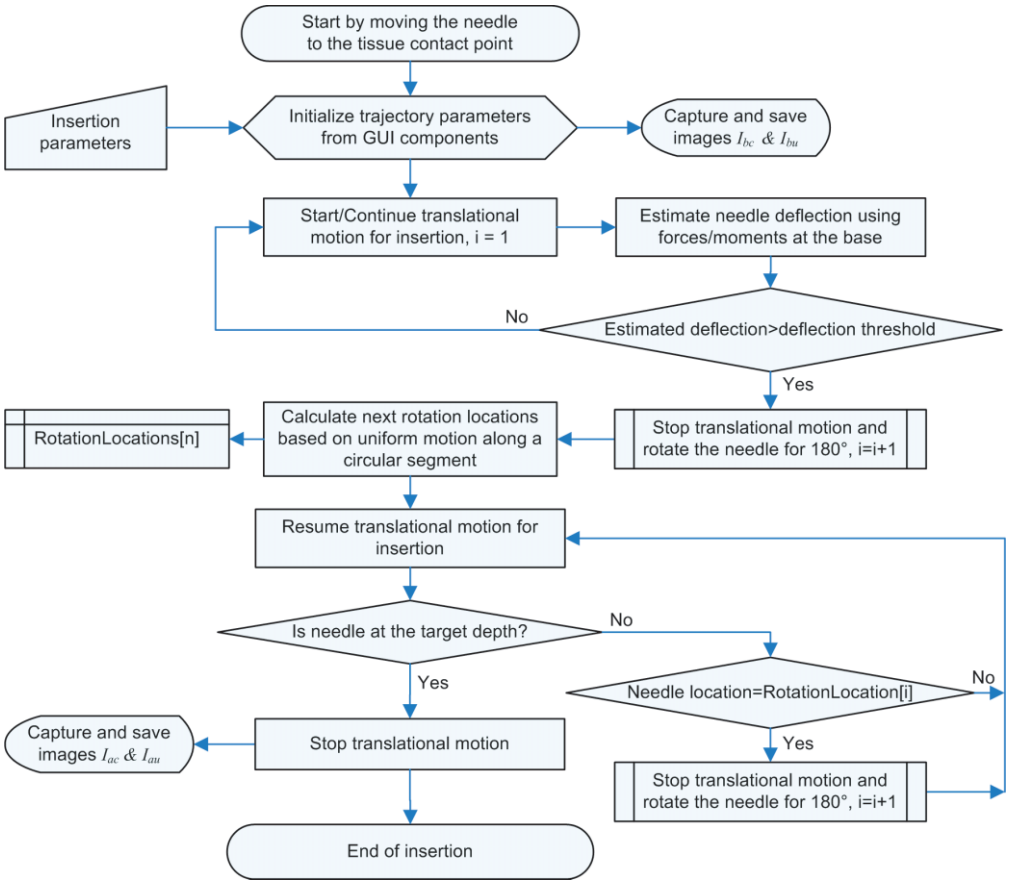

Figure 7. Flowchart of the trajectory-generation algorithm

plane of insertion, with one bead defined as the target in the image. Position of the target bead is calculated using I_{bu} and I_{au} and its displacement is considered to be equal to the amount of tissue deformation at the target (δ_{target}):

$$\delta_{target} = \|T_{US}T_C P_{bb} - T_{US}T_C P_{ba}\| \quad (10)$$

where T_C is the ultrasound calibration matrix, T_{US} is the transformation matrix of the ultrasound probe and P_{bb} and P_{ba} are pixel positions of the target bead in I_{bu} and I_{au}.. Pixel positions are defined as $[x, y, 0, 1]'$, where x and y define the row and column pixels of the target bead.

Results

Experiments were carried out on phantoms of beef muscle. The 20 cm cannula of a 18Ga surgical needle ($E = 200$ GPa, $G = 75$ GPa) with a 22° bevel was used for the experiments. Beads were made by cutting a stylet into 4 mm pieces. The needle was inserted with constant translational velocity of 10 mm/s. The 180° rotations were performed with constant rotational velocity of 5 r.p.m. The same downward-sloping orientation for the bevel at the point of entry into the tissue was used for all insertions.

The experiments were divided into three groups. The experiments in Group 1 validated the proposed needle deflection model. The experiments in Group 2 used the proposed needle deflection model and evaluated the effects of needle rotation on the overall amount of needle deflection, as well as tissue deformation at the tissue entry point and at a target. The experiments in Group 3 compared the effect of the following insertion methods on needle deflection: needle insertion with no rotation; needle spinning; and needle insertion using the proposed trajectory based on deflection model. It is important to note that each group of experiments was performed at different times with different tissues. Therefore, the results of each group should only be compared with the results within that group, as tissue properties can vary slightly. The results are presented as mean ± standard error of the mean (SEM).

The proposed model for estimating needle tip position was implemented in the NeedleController application. The estimated values were logged at the frequency of 10 Hz along with the actual 3D needle tip positions measured by a sensor coil. Six insertions were performed. In addition to beef muscle, the estimation model was also validated with the previously recorded data from six insertions into pig's heart. The results showed that the mean absolute error of estimation during a 60 mm insertion was 0.23 ± 0.01 mm for beef muscle and 0.24 ± 0.01 mm for pig's heart. Figure 8 shows the results of one insertion into both phantoms. The estimated amount of deflection at the tip, shown by the dashed lines,

DOI: 10.1002/rcs

was obtained using equation 7. Although in Figure 8 the needle tip position seems to follow a linear trajectory, the needle shape after insertion remains curved, due to tissue deflection at the entry point. Figure 9 describes the result of the measured and estimated amount of needle deflection at 30 mm and 60 mm depth for Group 1. The maximum estimation error during all insertions in both phantoms was 0.6 mm at the target.

The algorithm for estimating the needle tip position after rotations occur was implemented based on the needle's motion along the circular segment and the calculated radius of curvature (ρ) prior to the first rotation. The results showed that the mean absolute error of estimation during insertion with 180° needle rotations was 0.22 ± 0.01 mm for beef muscle.

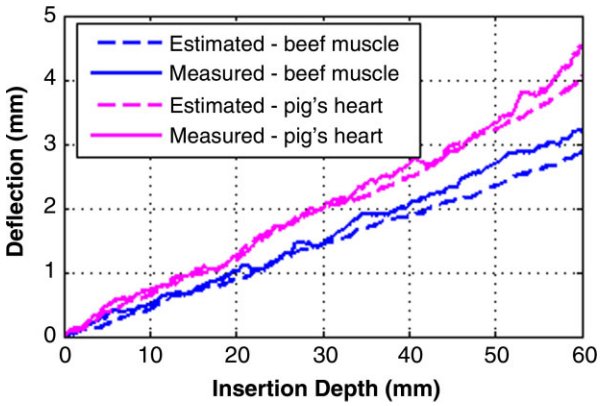

Figure 8. Estimated and measured needle deflection at the tip. The measured deflection is calculated from the measured position of the tip during insertion minus the measured position of the tip during insertion into air in each direction

After the accuracy of the needle deflection model had been validated, experiments in Group 2 were performed to study whether 180° needle rotation reduces the amount of needle deflection as conjectured. Twelve insertions were performed into each phantom: six insertions without needle rotation and six insertions based on the proposed trajectory. Prior to these experiments, a set of beads were placed orthogonal to the insertion direction for studying tissue deformation, as explained in the previous section. The deflection tolerance was set to 0.5 mm. In this study, trajectories were generated based on the uniform motion along a circular segment, where the constant radius of curvature was obtained from the average estimated radius prior to the first needle rotation (Figure 6, part A). To avoid the undesired increase of the needle deflection beyond the given threshold (Figure 6, part B), the algorithm for estimating the needle tip position after rotation was adjusted by reducing the threshold. Figure 10 shows the needle track in ultrasound images after one insertion using each method.

It is known that due to the elastic property of soft tissue, the tissue deforms during needle insertion and its deformation may cause target displacement. Although this study was initiated to minimize the amount of needle deflection and to keep the needle as straight as possible, we decided to investigate whether needle deflection affects the amount of tissue deformation. The amount of tissue deformation at the needle entry point to the tissue, δ_{entry}, for each of the above insertions was calculated.

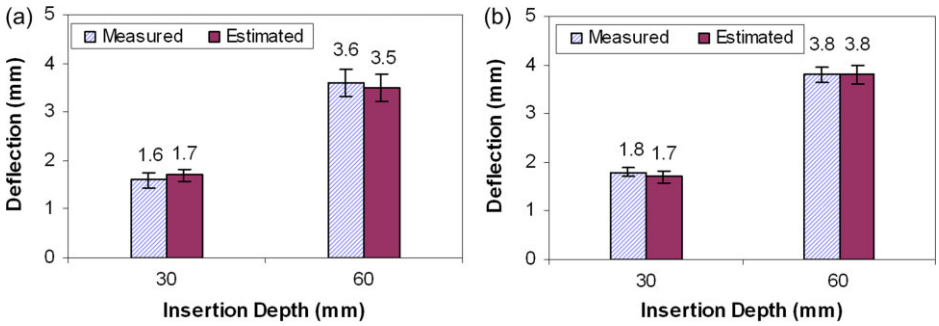

Figure 9. Measured and estimated needle deflection in (a) pig's heart and (b) beef muscle. Error bars show SEM ($n = 6$)

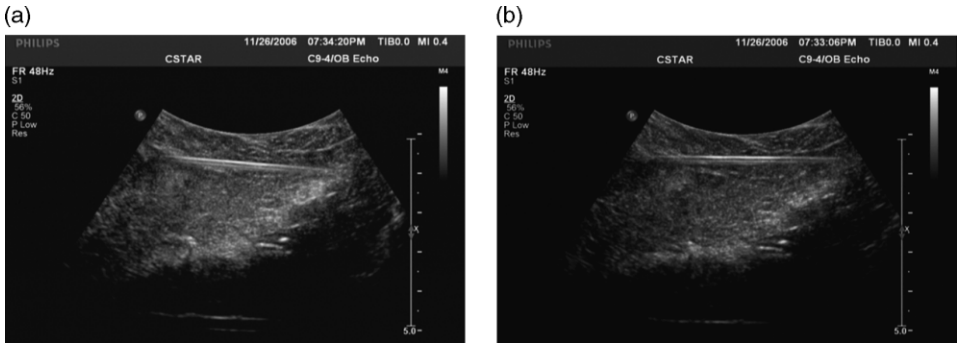

Figure 10. Ultrasound images after needle insertion: (a) insertion without rotation; (b) insertion using the proposed algorithm to minimize deflection

DOI: 10.1002/rcs

Table 1. Effect of the proposed trajectory on needle deflection and tissue deformation (n = 6)

Effect	Trajectory without rotation	Proposed trajectory	Achieved improvement (%)
Deflection at the target depth (mm)	3.1 ± 0.13	0.26 ± 0.07	91
Maximum overall deflection (mm)	3.1 ± 0.13	0.50 ± 0.03	83
Tissue displacement at the entry point (mm)	0.75 ± 0.07	0.26 ± 0.05	65
Tissue displacement at the target (mm)	10.35 ± 0.53	3.98 ± 0.34	61

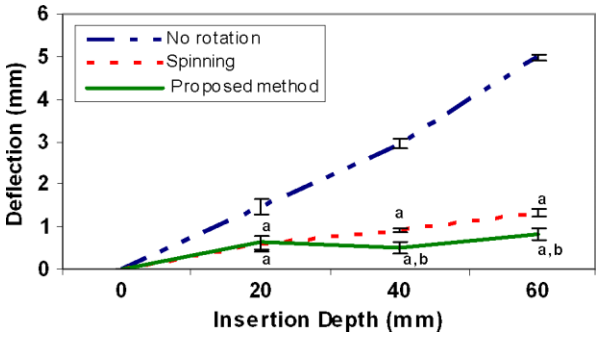

Figure 11. Needle deflection resulting from different insertion methods in beef muscle. ANOVA test showed that needle deflection at points labelled a and b are statistically different from the corresponding points in the methods with no rotation and with spinning, respectively. Error bars show SEM ($n = 6$)

It was observed that deflection at the entry point does not tear the tissue; rather, the tissue temporarily deforms because of its elastic property. In addition, the result of Euclidean measure of target displacement, δ_{target}, showed that minimizing needle deflection reduces target displacement. Table 1 summarizes the results of the proposed algorithm (Figure 7) for the experiments in Group 2. It was found that two rotations were required during insertion to minimize needle deflection in these experiments. The twisting angle was also measured during experiments into beef muscle. Its value never exceeded 0.52°.

The results of experiments in Group 3 are presented in Figure 11. In these experiments, six insertions were performed using each method. Needle spinning was generated at the rate of 50 r.p.m. A higher spinning rate could not be applied because of the wrap-around of the force sensor cable. The results show that the proposed method, based on online estimation of needle deflection, reduces the amount of needle deflection more than needle spinning.

Discussion

In this study, it was observed that the needle shaft had a curved path after insertion into soft tissue. However, the curvature of the path was different for different tissue types. The proposed algorithm has been developed for procedures where no imaging feedback is available and only one tissue type is involved. This study was initiated for use in the prostate brachytherapy procedure, in which multiple needles are to be inserted through the perineal skin. In this procedure, no imaging feedback is provided before a needle reaches close to the neighbourhood of the prostate gland. Extending this algorithm for other medical applications will require experiments to be performed on phantoms of multiple tissues. This is part of our ongoing study. The results obtained to date show that the non-homogenity in beef muscle due to the existence of fatty layers does not have any appreciable effect on the curvature of the needle's path.

The main advantage of this study was that the proposed model for estimating needle deflection does not require explicit knowledge of tissue properties. Therefore, variation of tissue properties in patients who undergo prostate brachytherapy would not significantly affect the accuracy of the algorithm. Moreover, an integrated online optimization strategy would allow the clinician to use the minimum deflection tolerance while maintaining constraint on the number of needle rotations (17).

We also implemented the model presented by Kataoka *et al*. (9) in order to compare with our estimation model. However, the results obtained from their model did not match the slope or the amount of the actual needle deflection. Kataoka *et al*. (9) suggested that the lack of another parameter, such as an additional moment or rotational component, could be the source of inaccuracy for their model.

Although we found that needle spinning shows a performance quite similar to our proposed method, there are a few factors which stand out in our method. First, needle spinning may cause tissue damage during insertion in soft tissue (11). This damage results from any small inaccuracy in the machining of the needle holder or any minor defect in the straightness of the needle. Any of these could reflect more at the tip, due to the length of the needle. In such circumstances, increasing rotational velocity would increase the damage. Second, high-rate needle spinning requires removal of the force/torque sensor from the needle holder, because of the wrap-around of the sensor cable. In some applications, it may be acceptable to remove the sensor. However, in many medical applications, the presence of a force/torque sensor in needle assembly could improve other aspects of insertion, such as detection of transition between tissue layers, parameter estimation and/or controlling tissue deformation (1). Wireless force/torque sensors should also prove useful. Finally, it is clear that high-rate needle spinning cannot be achieved in manual needle insertions. Therefore, needle spinning is only suitable for cases when a robot-assisted insertion is performed. However, our proposed method can be used for manual insertions and

can be implemented as a computer-assisted method, using a needle holder equipped with a force/torque sensor. During manual insertion, the program defines when rotation is required and feedback can be provided to the clinician via a software user interface or a hardware indicator, such as a light-emitting diode (LED) on the needle holder.

Concluding Remarks

This research was carried out to find a model that can be used to estimate the amount of needle deflection in soft tissue, in order to compensate for it. Needle insertions were performed on different tissues and the relationships between force/torque readings at the needle base, insertion depth and needle deflection for a bevelled-tip needle were investigated. Estimation of needle deflection intraoperatively can be used to update needle insertion trajectories, by rotating the needle through 180° to compensate for the deflection. Our needle-deflection model estimated the amount of needle deflection with high accuracy during insertion into soft tissue. The results showed a significant reduction in needle deflection along the needle path when the trajectory was updated. The average deflection error at the target depth was reduced by about 90%, while tissue deformation at the target was also reduced. This study presented a method that is particularly suitable for situations where needle insertions are to be performed using a robotic system, since it requires precise needle rotations. The results of this study can improve the accuracy of needle insertions in robot-assisted prostate brachytherapy prior to the appearance of the needle tip in the ultrasound field of view. Our ongoing work is concerned with integration of this algorithm with real-time imaging in order to precisely control needle motions close to the neighbourhood of a target inside the prostate.

Acknowledgements

This work was supported by the Natural Sciences and Engineering Research Council (NSERC) of Canada under Collaborative Health Research Project (CHRP) Grant No. 262583-2003, Discovery Grant No. RGPIN-1345, and by infrastructure grants from the Canada Foundation for Innovation and the Ontario Innovation Trust, awarded to CSTAR and the University of Western Ontario. Financial support for N.A. was provided by an NSERC Postgraduate Scholarship.

References

1. Abolhassani N, Patel RV, Moallem M. Needle insertion into soft tissue: a survey. *Med Eng Phys* 2006; **29**: 413–431.
2. Nath S, Chen Z, Yue N, Trumpore S, Peschel R. Dosimetric effects of needle divergence in prostate seed implant using ^{125}I and ^{103}Pd radioactive seeds. *Med Phys* 2000; **27**(5): 1058–1066.
3. Gupta P, Mordin C, Curtis J, *et al*. Pulmonary arteriovenous malformations: effects of embolization on right-to-left shunt, hypoxemia, and exercise tolerance in 66 patients. *Am Roentgen Ray Soc* 2002; **179**: 109–112.
4. Maher MM, Gervais DA, Kalra MK, *et al*. The inaccessible or undrainable abscess: how to drain it. *RadioGraphics* 2004; **24**: 717–735.
5. Mozer P, Leroy A, Payan Y, *et al*. Computer-assisted access to the kidney. *Int J Med Robotics Comput Assist Surg* 2005; **1**(4): 58–66.
6. Sun D, Willingham C, Durrani A, *et al*. A novel end-effector design for robotics in image-guided needle procedures. *Int J Med Robotics Comput Assist Surg* 2006; **2**: 91–97.
7. Trejos AL, Lin AW, Pytel MP, Patel RV, Malthaner RA. Robot-assisted minimally invasive lung brachytherapy. *Int J Med Robotics Comput Assist Surg* 2007; **3**: 41–51.
8. Okamura AM, Simone C, O'Leary MD. Force modelling for needle insertion into soft tissue. *IEEE Trans Biomed Eng* 2004; **51**(10): 1707–1716.
9. Kataoka K, Washio T, Audette M, Mizuhara K. A model for relations between needle deflection, force, and thickness on needle insertion. Proceedings of Medical Image Computing and Computer-Assisted Intervention Conference, Utrecht, The Netherlands, 2001; 966–974.
10. Abolhassani N, Patel RV, Moallem M. Control of soft tissue deformation during robotic needle insertion. *Minim Invasive Ther Allied Technol* 2006; **15**(3): 165–176.
11. Wan G, Wei Z, Gardi L, Downey D, Fenster A. Needle steering for 3D TRUS-guided robot-aided brachytherapy. Proceedings of the Computer Assisted Radiology and Surgery Congress, Chicago, IL, USA, 2004; 1325.
12. DiMaio SP, Salcudean SE. Needle steering and model-based trajectory planning. Proceedings of Medical Image Computing and Computer-Assisted Intervention Conference, Montreal, Canada, 2003; 33–40.
13. DiMaio SP, Salcudean SE. Needle steering and motion planning in soft tissue. *IEEE Trans Biomed Eng* 2005; **52**(6): 965–974.
14. Webster RJ III, Kim JS, Cowa NJ, Chirikjian GS, Okamura AM. Nonholonomic modelling of needle steering. *Int J Robotics Res* 2006; **25**(5–6): 509–525.
15. Alterovitz R, Branicky M, Goldberg K. Constant-curvature motion planning under uncertainty with applications in image-guided medical needle steering. Workshop on the Algorithmic Foundation of Robotics (WAFR), New York, 16–18 July 2006.
16. Gere JM. *Mechnics of Materials*, 5th edn. Brooks/Cole: Pacific Grove, CA; 2001.
17. Abolhassani N, Patel RV. Minimization of needle deflection in robot-assisted prostate brachytherapy. Proceedings of the Computer Assisted Radiology and Surgery Congress, Osaka, Japan, 2006; 269–271.
18. Zhang H, Banovac F, White A, Cleary K. Freehand 3D ultrasound calibration using an electromagnetically tracked needle. Proceedings of SPIE Medical Imaging Symposium, 2006; 775–783.